RESEARCH ARTICLE | AUGUST 06 2025

Regularization of a conceptual model for Dansgaard–Oeschger events

Special Collection: Nonautonomous Dynamics in the Climate Sciences

Bryony Hobden ; Peter Ashwin ; Paul D. L. Ritchie

Chaos 35, 083114 (2025)
https://doi.org/10.1063/5.0244302

Regularization of a conceptual model for Dansgaard–Oeschger events

Cite as: Chaos 35, 083114 (2025); doi: 10.1063/5.0244302
Submitted: 17 October 2024 · Accepted: 21 July 2025 ·
Published Online: 6 August 2025

Bryony Hobden,[a] Peter Ashwin, and Paul D. L. Ritchie

AFFILIATIONS

Department of Mathematics and Statistics, University of Exeter, Exeter EX4 4QF, United Kingdom

Note: This paper is part of the Focus Issue, Nonautonomous dynamics in the climate sciences.
[a]**Author to whom correspondence should be addressed:** B.Hobden@exeter.ac.uk

ABSTRACT

The Dansgaard–Oeschger events are sudden and irregular warmings of the North Atlantic region that occurred during the last glacial period. A key characteristic of these events is a rapid shift to warmer conditions (interstadial), followed by a slower cooling toward a colder climate (stadial), resulting in a saw-tooth pattern in regional proxy temperature records. These events occurred many times during the last 100 000 years and have been hypothesized to result from various mechanisms, including millennial variability of the ocean circulation and/or nonlinear interactions between ocean circulation and other processes. Our starting point is a non-autonomous, conceptual, but process-based, model of Boers *et al.* [Proc. Natl. Acad. Sci. **115**, E11005–E11014 (2018)] that includes a slowly varying non-autonomous forcing represented by reconstructed global mean temperatures. This model can reproduce Dansgaard–Oeschger events in terms of shape, amplitude, and frequency to a reasonable degree. However, the model of Boers *et al.* has instantaneous switches between different sea-ice evolution mechanisms on crossing thresholds and, therefore, cannot show early warning signals of the onset or offset of these warming events. In this paper, we regularize this model by adding a fast dynamic variable so that the switching occurs smoothly and in finite time. This means the model has the potential to show early warning signals for sudden changes. However, the additional fast timescale means these early warning signals may have short time horizons. Nonetheless, we find some evidence of early warning for the transition between slow and rapid cooling for the model.

Dansgaard–Oeschger (DO) events are abrupt temperature changes that occurred during the last glacial period (110-10 thousand years ago). Although felt worldwide, they were most pronounced in the North Atlantic region. A DO cycle consists of a DO event (a rapid and abrupt warming) followed by a warm interstadial period, a cooling, and finally a colder stadial period. There are competing explanations for the drivers of these cycles. It is not known whether this is entirely due to millennial-timescale variability of the Atlantic Meridional Overturning Circulation (AMOC) or due to a system-level interaction between different climate system components, such as sea ice, AMOC, and atmosphere. There is also an ongoing debate in the literature regarding their predictability. The conceptual model we investigate here is a regularization of a model of Boers *et al.* [Proc. Natl. Acad. Sci. 115, E11005–E11014 (2018)]. This uses sea ice and ocean circulation interactions to produce behavior similar to that of the proxy temperature record for DO events during the last glacial period. For this model, we attempt to identify, with partial success, early warning signals for abrupt changes associated with the start and end of DO events.

I. INTRODUCTION

A significant development in understanding the climate of the last 100 000 years was the discovery in the 1980s of repeated rapid changes in climate within the oxygen isotope records from Greenland ice cores.[1–5] The signals of these "Dansgaard–Oeschger" (DO) events have since been found to be present globally and have occurred many times during the cold period of the last glaciation.[6,7] The DO events occur within a "DO cycle" that follows a pattern of relatively rapid warming (with temperature rises between 5 and 16.5 °C for single DO events[8]) and cooling between the interstadial and stadial phases. While signals of DO events are observable even

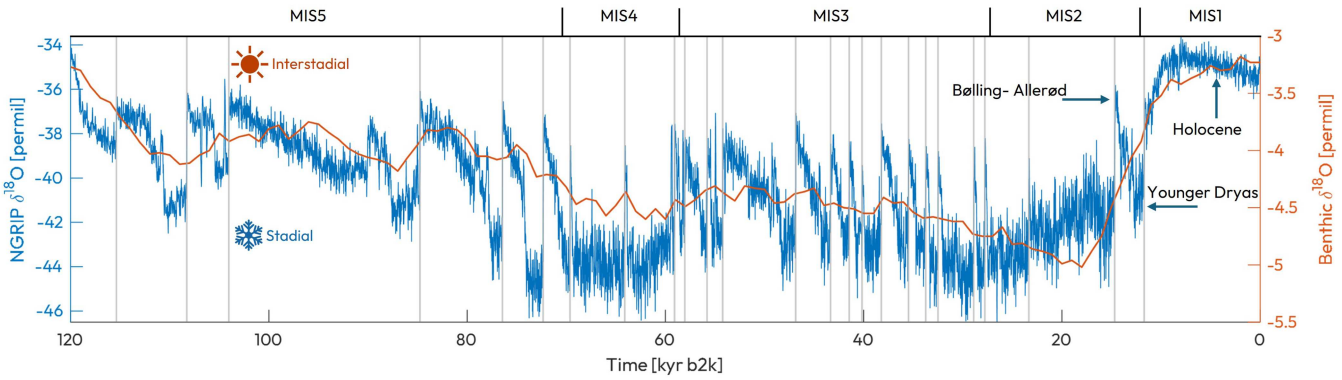

FIG. 1. Variability of the stable oxygen isotope ratio (δ^{18}O) during the last glacial period. In this figure and throughout the paper, kyr b2k refers to "millennia before the year 2000." The blue line indicates the Northern Greenland Ice Core Project (NGRIP) δ^{18}O data with regular sampling of 20 years.[9] The ratio of stable oxygen isotopes ^{16}O and ^{18}O (δ^{18}O) is often used as a proxy for atmospheric temperature at the site of the ice core, with more negative values indicating colder temperatures and less negative values indicating warmer temperatures. The orange line is the benthic record[10] of δ^{18}O, which is a proxy for total global ice volume and, thus, a proxy for the background global mean temperature. Thin gray lines indicate the observed DO events. Marine Isotope Stages (MISs) are indicated at the top of the figure.

in Antarctica, DO events are primarily located in the North Atlantic region. Figure 1 shows a proxy record from the Northern Greenland Ice Core Project (NGRIP) drilling site that has been mapped onto a time series showing δ^{18}O vs time.[9] The NGRIP record is shown together with a more slowly varying benthic ocean record stack for $\delta^{18}O$, which is a proxy of average ice volume (and hence global temperatures).[10]

Various studies have identified variability of the AMOC occurring on timescales up to millennia[11–13] and a productive line of modeling suggests that DO events emerged from such millennial-timescale instability of ocean circulation, through changes in the North Atlantic Meridional Overturning Circulation (AMOC) associated with salinity feedback.[14–16] The extent of Arctic sea ice has been postulated to play a role in forced millennial oscillations. Ocean–atmosphere–sea ice coupled models have shown that during glacial intervals, sea ice extent shifts southward,[17,18] which coincides with a southward shift of the AMOC. One hypothesis is that the displacement of the AMOC with respect to the mean atmospheric field[19] makes the system unstable and leads to the millennial variability.[16] A more widespread explanation for DO cooling events is that advancing sea ice interrupts the atmosphere–ocean heat flux and, in addition to that, freshens the surface layer upon melting.[20–23] Both of these mechanisms act to inhibit the deep convection, which is required to fuel the AMOC's lower limb.

It is a topic of active research to understand the process interactions that give rise to DO events in IPCC-class Earth System Models (ESMs) and to understand their timing and predictability.[20,21,24–26] It has been suggested that the abrupt changes may result from the interaction of several nonlinear climate elements.[27] Starting with Peltier and Vettoretti,[28] a range of recent large-scale models can reproduce rapid changes in North Atlantic temperature for a range of atmospheric CO_2 levels similar to those during the last glacial period[29]—a recent comprehensive review of DO-type events in ESMs is in Malmierca-Vallet *et al.*[20] There it was concluded that the configurations that are conducive for a variety of ESMs to display DO-type behavior are low obliquity levels, medium to low CO_2 concentrations during the Marine Isotope Stage 3 period, relatively small Laurentide ice sheet that causes changes to the Northern Hemisphere atmospheric circulation and results in a weak AMOC, and potentially greater sea ice. However, it is unfeasible for high-resolution ESMs to be run for long enough durations to determine their capability of simulating DO-type behavior.

For the latter research, several lower-order "conceptual models" have been proposed to understand the aspects of DO oscillations. These include a variety of process-interaction inspired models, Vettoretti *et al.*,[30] Riechers *et al.*,[31] Gottwald,[32] Timmermann *et al.*,[33] Singh *et al.*,[34] Melcher *et al.*,[35] and Schulz *et al.*[36] are a selection. Models need to include a range of timescales to have the potential to show abrupt changes. The model we consider is that of Boers *et al.*,[37] which assumes that DO events involve interactions between the AMOC, Arctic sea ice extent, and ocean temperatures.[22,29,38] As we highlight in Sec. II, this model has singular behavior in the form of threshold switching that we remove by introducing a fast dynamic variable that regularizes[39] the model. In other studies, the term "desingularize" is sometimes used to mean "regularize." Regularizing the model opens up the possibility for early warning signals (EWS) to be detectable, ahead of abrupt transitions, which is not possible in the original model of Boers *et al.*[37] as there is no loss of stability on switching.

There have been various attempts to identify statistically significant EWS of different DO events. Tipping points can appear when a parameter for a subsystem slowly passes through a fold bifurcation. Under such an assumption, the phenomenon of critical slowing down is expected, typically detected through statistical early warning signals that include observing an increase in variance and autocorrelation of the signal as the tipping point is approached.[40]

An increasing trend in the autocorrelation, which suggests a destabilization of the system dynamics and hence approach to an underlying fold bifurcation, has been found leading up to the end of the Younger Dryas period and Bølling–Allerød transition.[41,42] EWS are never perfect; assessing the time-local variance and autocorrelation requires sufficiently long periods.[26,43,44] Detecting critical slowing down also crucially depends on the observable, specifically selecting the correct observable to look for critical slowing down[45] and for that observable to have sufficient resolution.

Analysis in high-periodicity bands (i.e., 40–60 years) can show statistically significant increases in the scale-averaged wavelet coefficients (ω^2, an estimator of the variance) when an ensemble of DO events was considered, using 20 year mean data of the NGRIP record. When individual events were looked at, only two events showed statistically significant increases in variance preceding the DO onset.[46] Intuitively, one may assume that the ensemble average would smooth out the time series fluctuations, and hence make it harder to see an increase in the variance. However, it is noted in Boers[42] that the increase in variance in the ensemble average is dominated by the transition to the Bølling–Allerød interstadial. It should also be noted that the Bølling–Allerød transition is one of the only DO events that, when analyzed on its own, showed a significant increase in variance.

The theory of critical slowing is based on an increase in both autocorrelation and variance.[43] Since the study by Rypdal[46] did not look at the ensemble autocorrelation, one cannot conclude whether there is an underlying bifurcation associated with critical slowing down, and it still leaves the possibility that these abrupt transitions are noise-induced. Another possible explanation is that an observed substantial rise in variance may merely reflect a higher level of noise. In an analysis of a higher resolution NGRIP ice core record, statistically significant variance and autocorrelation were found in the high-frequency bands, suggesting a physical mechanism for DO events operating on fast time scales.[42]

The majority of studies involving EWS and DO cycles have looked at DO onsets (i.e., the transition from stadial to interstadial conditions).[15] Since a key signature of DO cycles also includes a rapid transition from warm to cold conditions, it might prove enlightening to also look at the statistical early warning signals for a DO offset (the transition from interstadial to stadial). Recently, robust early warning signals for interstadial periods generally longer than 1500 years have been found, but little evidence of EWS for interstadials shorter than this.[47]

Dust proxy records have been used to suggest that DO event onsets and offsets cannot be produced by noise-induced transitions alone, although noise may in part explain the variability in stadial and interstadial timescales.[48] Using the ensemble mean of the early warning signals for the DO events provides moderate but significant increases in variance and autocorrelation in the time period of 1800–250 years before the tipping event.[49] This approach clearly cannot be used for the prediction of abrupt shifts, but it is a technique that can provide a better understanding of the underlying mechanisms causing them. Similarly, Ditlevsen and Johnsen[50] looked at the ensemble mean of the statistical indicators for EWS, but for a shorter period preceding the transition (900 years before the tipping event) and found no statistically significant trend. This led the authors of the study to conclude that DO events are examples of noise-induced transitions and, therefore, offer little predictability. However, this method does not acknowledge the potential for some DO events to be noise-induced and others to be bifurcation-induced tipping events. A drawback of looking at the ensembles rather than the individual events is that a large amount of noise in one event may obscure the EWS that might be present in some of the individual events.

Some studies have hypothesized that DO events could be indicative of crossing a homoclinic bifurcation, and therefore it is unclear if critical slowing down would still be present.[51,52] Another possible reason for the lack of skill of predictability of DO events over longer timescales is associated with millennial variability of a chaotic trajectory.[53,54] In short, there is a rich but inconclusive literature on the dynamical mechanisms and predictability of DO events.

If EWS are present, one may conclude that DO events are indeed bifurcation-induced. However, this does not answer which climate element undergoes the bifurcation and in which proxy records we can observe it. A good model of DO events should reproduce EWS if present. Conceptual models may help us to understand how the different climate components can be coupled such that one can undergo repeated bifurcations to shift the entire system to a different regime. The conceptual model may then inform the ESM analysis of DO cycles.

The model of Boers *et al.*[37] shows sequences of simulated DO events with frequencies similar to the observed DO events. However, the nature of their model means that a precursor signal will not be visible in the noise response: rather than instability, the switching occurs when a threshold is hit. For this reason, we aim in this paper to develop a regularized version of the model of Boers *et al.*[37] By regularizing a continuous-time dynamical system with instantaneous switching,[39,55] we create a system that is limited to the switching system as some timescale ratio approaches zero. We replace the assumption of singular and instantaneous switching between different evolutionary processes for the sea ice extent C with a fast dynamical system that exhibits tipping between three different stable branches. We aim to make redefining of this "ice regime process" that was hidden in Boers *et al.*[37] visible in our model.

The paper is organized as follows. In Sec. II, we describe our regularization of the model from Boers *et al.*[37] Section III presents simulations using this non-autonomous model to verify that our model can capture DO events to a similar extent as Boers *et al.*[37] In Sec. IV, we use the regularized model to examine early warning signals for tipping between the different phases of the DO cycle in our model. Unlike in the model of Boers *et al.*,[37] we can find some early warning signals for a transition from interstadial to stadial, but they are limited by the timescale of the fast system. The transition from stadial to interstadial is less clear. In Sec. V, we conclude with a discussion of some implications and deficiencies of this study.

II. REGULARIZING A CONCEPTUAL MODEL OF DANSGAARD–OESCHGER EVENTS

In this section, we regularize the conceptual model for DO events presented in Boers *et al.*[37] This is a non-autonomous, stochastic, nonlinear model with variables: sea ice extent in the North Atlantic C, the atmospheric temperature over Greenland T_G, the

subsurface water temperature in the North Atlantic T_{NAW}, and the Atlantic Meridional Overturning Circulation strength anomaly ψ (which we interpret as being relative to some fixed reference strength ψ_0). We introduce an additional variable λ that represents fast processes that regularize the instantaneous switching between different modes of evolution of sea ice in the original model. We do not have a clear physical interpretation of λ but suggest it may represent a combination of circulation and ice dynamics, for example, grounding and buttressing that are associated with the instantaneous switching hypothesized by Boers *et al.*[37]

One of the focuses of Boers *et al.*[37] is to show how the coupling between the ocean circulation and the isotope ratio can produce the bi-polar see-saw effect observed in Greenland and Antarctic δ^{18}O isotope ratios, but in this paper, we choose to focus on the Greenland isotope ratios solely, and we do not include an equation for the isotope ratio in Antarctica.

The equations suggested by Boers *et al.*[37] for the evolution of T_G, T_{NAW}, and ψ are as follows:

$$\dot{T}_G = -p_0\left(T_G - T_G^*(t)\right) + 10p_0 T_{NAW}\Theta(T_{NAW})(1-C), \tag{1}$$

$$\dot{T}_{NAW} = -p_0\left(T_{NAW} - T_{NAW}^*(t)\right) - 10p_0 T_{NAW}\Theta(T_{NAW})(1-C) - p_0\psi, \tag{2}$$

$$\dot{\psi} = \psi - \psi^3 - p_0\left(T_{NAW} - \frac{\tau}{2}\right). \tag{3}$$

This model relies on internal feedbacks between the ocean circulation, sea ice extent, and subsurface water temperature to produce self-sustaining DO-type oscillations. The subsurface water temperature in the North Atlantic T_{NAW} affects the atmospheric temperature over Greenland T_G. These two variables are coupled so that oceanic-atmospheric heat transport happens at a magnitude faster than the rest of the dynamics. The parameter $p_0 = 5.56$ determines how fast each variable is pulled back to its respective fixed point and is taken directly from Ref. 37.

Boers *et al.*[37] assume that the process is dependent on the evolution of a variable $0 \le C \le 1$ representing the sea ice extent, such that $C = 1$ represents a full sea ice extent and $C = 0$ represents a complete loss of sea ice in the North Atlantic. The Heaviside function $\Theta(x)$ prevents atmospheric-oceanic heat transport from happening if the water temperature drops below 0 °C. In their model, the sea-ice cover effectively evolves according to

$$\dot{C} = \begin{cases} s_1 & \text{if } 0 \le C < \bar{C} \text{ and } T_{NAW} < \tau, \\ s_2 & \text{if } \bar{C} \le C < 1 \text{ and } T_{NAW} < \tau, \\ 0 & \text{if } C = 1 \text{ and } T_{NAW} < \tau, \\ -\infty & \text{if } C > 0 \text{ and } T_{NAW} \ge \tau. \end{cases} \tag{4}$$

Note that C grows to $C = 1$ in two stages but then jumps discontinuously to $C = 0$ when T_{NAW} exceeds $\tau = 10$ °C; $s_1 > 0$ represents the initial slow growth rate of C, which is also taken as a function of the background global mean temperature as represented by benthic $\delta^{18}O$. This is followed by a faster growth rate $s_2 > 0$ on reaching a threshold $\bar{C} = 0.5$.[37] Here, s_2 is a constant chosen by Boers *et al.*[37] to ensure that sea ice cover increases rapidly from $C = 0.5$ to $C = 1$.

Equation (3) permits two stable states for the AMOC, during interstadials, the overturning circulation ψ is in a strong state, which transports warm, salty surface water from the equator toward the North Atlantic.

In this model, a lack of sea ice cover allows for greater oceanic-atmospheric heat exchange and, thus, subsurface temperatures in the North Atlantic T_{NAW} are lower, despite the continuous strong supply of warm surface waters by the AMOC, and atmospheric temperatures over Greenland T_G are high. During stadials, the converse is true. The overturning circulation ψ is in the weak state, and so there is less transportation of warm waters to the high northern latitudes. This permits a large sea ice extent in the North Atlantic to inhibit oceanic-atmospheric heat exchange, and thus atmospheric temperatures over Greenland T_G decrease, and subsurface water temperatures T_{NAW} increase and build up below the sea ice. This then further inhibits deep water formation and keeps AMOC in a weak state.

Note one could argue that the effect of ψ on T_{NAW} should have the opposite sign, but we leave this to be consistent with Boers *et al.*[37] and note that simulations are not qualitatively changed by doing this. The strength of the AMOC is represented using a model of Cessi[56] with a cubic nonlinearity—this is a simplification of the Stommel model[57] and has bistability. The functions $T_G^*(t)$ and $T_{NAW}^*(t)$ that appear in Eqs. (1) and (2) are assumed to depend only on global mean temperature; hence, they are assumed to be low-pass filtered and linearly scaled versions of the benthic δ^{18}O isotope ratio curve $B(t)$.[42] As in the original model of Boers *et al.*, the variables T_G and T_{NAW} are assumed to relax toward $T_G^*(t)$ and $T_{NAW}^*(t)$, respectively, in the absence of other effects. The time series $T_G^*(t)$ and $T_{NAW}^*(t)$ have been filtered and linearly scaled in the same way as in Boers *et al.*[37]

We aim to regularize the switching process for C represented in (4) by introducing an additional fast variable λ and noise as follows. We suppose that C and λ evolve according to

$$\begin{aligned} dC &= h(\lambda, B, C)(\lambda - e^{2(C-a)})dt, \\ d\lambda &= \frac{1}{\epsilon}g(\lambda, C)dt + \sigma\, dW, \end{aligned} \tag{5}$$

where $g(\lambda, C)$ is a function that gives at most three stable regimes of the behavior of λ for certain values of C, and such that there are tipping points between these ranges that model the instantaneous transitions in Boers *et al.*[37] The functional form we use for g and the rationale for this is described in Appendix A. Note that Eqs. (1)–(3) are now formally SDEs if we consider (5), though for simplicity we only consider stochastic forcing of the fast component λ.

We set

$$a = \frac{2 - \ln(2)}{2} + 0.01(T_{NAW} - 10), \tag{6}$$

so that the nullcine for C varies with T_{NAW}. Moreover, we set $h > 0$ by

$$h(\lambda, B, C) = \begin{cases} 12.5 & \text{for } \lambda \le -1, \\ f(B) & \text{for } -1 \le \lambda < 1.5 \ \&\ C < 0.6, \\ 5 & \text{otherwise.} \end{cases} \tag{7}$$

Here, $f(B)$ denotes a random sample from a 2D Gaussian kernel density estimate (KDE) of the joint density between speed (taken as the inverse of the interstadial duration) and benthic δ^{18}O, as in

Boers *et al.*[37] (see Appendix). In the KDE, speeds range between 0 and 5/kyr, and hence we assign sea ice growth to the fastest growth speed $h = 5$ for sufficiently cold benthic values ($B < -4.7933$). The function h is set to ensure that the timescales of the regimes are comparable to those in Boers *et al.*[37] while ϵ is small (so that the tipping points are rapid). More precisely, the timescale ϵ is taken to be $\epsilon = 0.01$ kyr, meaning that C is a slow variable and λ is a fast variable in the system (5).

The system (1)–(3) together with (5) is a fast–slow dynamical system where λ is a fast variable that encodes different stable sea ice configurations in analogy to (4). Note that λ evolves according to a stochastic differential equation with Wiener noise W of amplitude σ. This is numerically solved using an improved Euler (Heun) scheme.[58] The fast–slow dynamical system has three slow stable manifolds corresponding to different sea ice growth rates to produce the three different regimes observed in the NGRIP isotope record as shown in Fig. 2: (a) slow initial cooling during the interstadial associated with the slow growth of the ice shelf, (b) rapid cooling associated with an increase in sea ice extent and transition to stadial conditions, and (c) rapid warming from stadial to interstadial conditions associated with retreat of sea ice and destabilization of the ice shelf.[37] The form of g in Eq. (A1) has been chosen to produce the desired slow manifolds (see Appendix A). A summary of model parameters can be found in Table I in Appendix B.

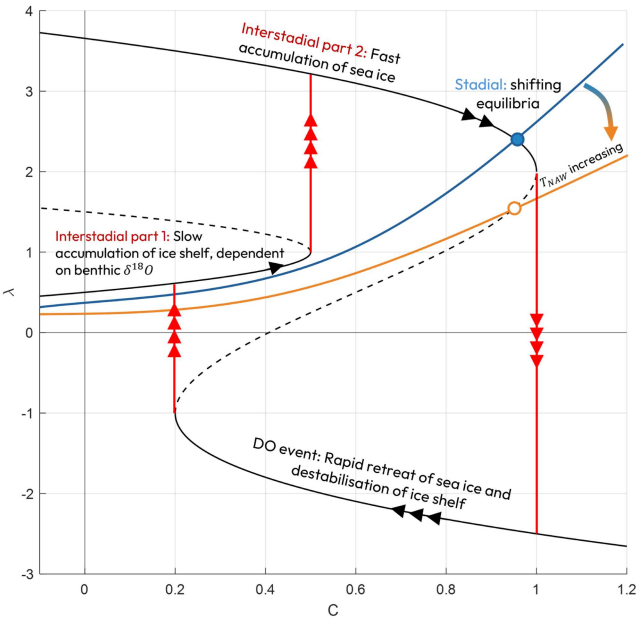

FIG. 2. Black: λ nullcines for Eq. (5) in the noise-free case, $\sigma = 0$. Possible nullcines of C are plotted in blue and orange depending on the value of T_{NAW}. Filled points and empty points correspond to stable and unstable equilibria, respectively. Superimposed in red is a trajectory of the singular system, $\epsilon \to 0$ as in Eq. (5) in the noise-free case. The λ nullclines correspond to the stable and unstable manifolds of the slow–fast system in Eq. (5), shown by the solid and dashed black lines, respectively. Each stable manifold corresponds to one of the three stable ice regimes. The arrows indicate the relative speed at each point in the DO oscillation, such that the black arrows (specified by h) indicate the relative speeds at which the system moves along each slow manifold and the red arrows indicate the direction and relative speed of the fast dynamics in the λ direction.

The model of Boers *et al.*[37] assumes that the sea ice extent C evolution abruptly switches between regimes, as expressed in (4). Our regularization using the fast variable λ expresses this evolution using the function $h(\lambda, B, C)$ that sets ice shelf/sea ice growth speed. When the system is in the slow cooling phase associated with the ice shelf reformation, f is randomly sampled from a Kernel Density function of speed and benthic $\delta^{18}O$. Many studies have identified an inverse relationship between the length of the interstadial period and the background global mean temperature.[31,32,37] Hence, we assume the speed of ice shelf reformation is the inverse of interstadial duration and create a Kernel Density Estimation of benthic $\delta^{18}O$ against speed, as in supplementary information of *et al.*[37] (see Appendix C). For sufficiently negative λ, we set h to be relatively large, creating a rapid retreat in sea ice, which we associate with the onset of a DO event (see Fig. 2).

We explicitly introduce a dependence of sea ice extent growth on the subsurface water temperature in the North Atlantic. As T_{NAW} varies between approximately 0 and 20 °C (temperatures will typically be a lot lower in reality), a varies, which in turn alters the evolution of C. This intuitively makes sense; when the subsurface water temperature in the North Atlantic is high, this will have some effect (mostly negative) on the state of the sea ice; the opposite is also true. This model operates under the idea that when the subsurface water temperature in the North Atlantic is too high, this will destabilize the sea ice and ice shelf from underneath, causing the opening of large polynya,[25,29] from which the sea ice cannot recover, as illustrated schematically in Fig. 3. This, too, was the physical process motivating the model in Boers *et al.*;[37] however, this effect was achieved by a constraint in the computation such that when T_{NAW} reached a critical threshold, the sea ice extent was set to $C = 0$. The main difference here is that we have introduced a fast variable such that the switches between the different sea ice growth phases are caused by smooth transitions of the fast–slow dynamical system. There are some aspects of the original model of Boers *et al.*[37] that are clearly oversimplifications—for example, we do not take into account the effect of T_g on C, and one could argue that the sign of p_0 in Eq. (2) is incorrect. We do not attempt to correct these in this work, but focus on the regularization of the existing model.

The variable we use to compare against the NGRIP isotope record is the stable oxygen isotope ratio, I_G,

$$I_G(t) = I_G^*(t) + 0.01T_G + 4.32(1 - C(t)) - \beta\lambda(t), \qquad (8)$$

where β is a scaling parameter which we set to unity to include some influence of the variability of λ on I_G. $I_G^*(t)$ is a scaled and filtered vision of the benthic $\delta^{18}O$ time series, whereas Boers *et al.*[37] sets I_G^* to a constant estimated directly from the NGRIP record. This is the form of the equation as used in Boers *et al.*,[37] with the additional term corresponding to the fast variable. Lower values of I_G correspond to colder conditions. It is important to note that the concentration of $\delta^{18}O$ in Greenland ice cores is not a direct proxy for local temperature, but rather a proxy for the temperature gradient between the source of evaporation and the site of precipitation.[59,60] Analysis of the deuterium excess, defined as $d = \delta D - 8\delta^{18}O$, indicates a cooling of the moisture source at the onset of DO events.[61]

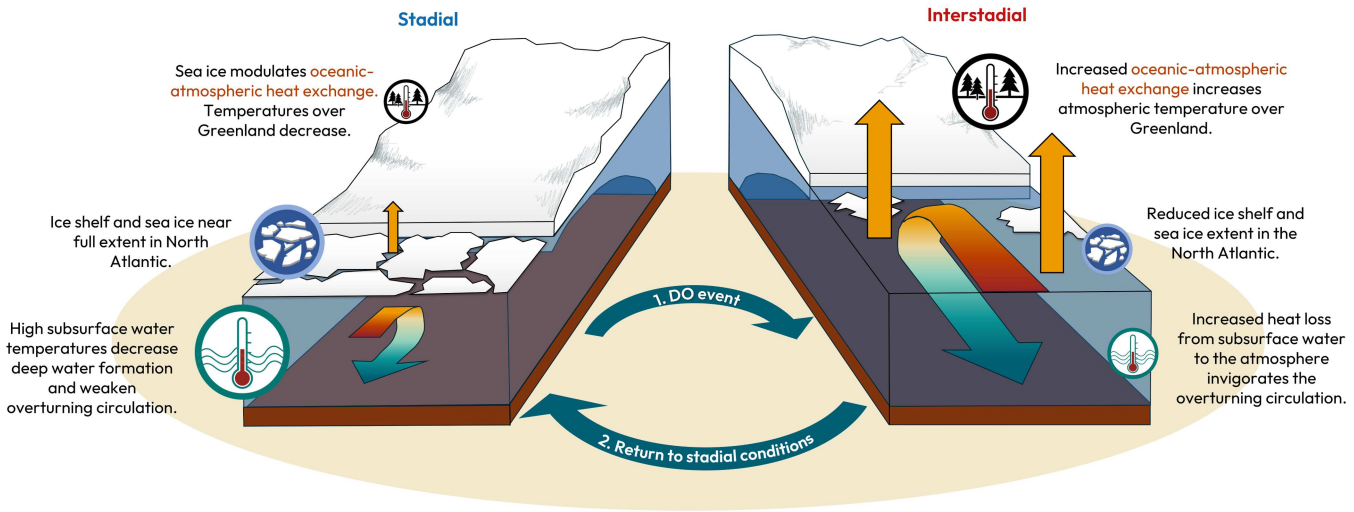

FIG. 3. Schematic of the mechanism in the model of Boers *et al.*[37] for Dansgaard–Oeschger events. Arrow 1 indicates the transition from stadial to interstadial conditions, which is the DO event itself. After a prolonged period of great sea ice extent in the North Atlantic (stadial), subsurface water temperatures become high enough to destabilize the sea ice and ice shelf from below, opening up large polynya, which leads to a rapid decrease in sea ice extent. Arrow 2 indicates the interstadial to stadial transition. Our regularized model includes a fast variable λ that switches between three different regimes of ice growth.

During DO events, Atlantic sea ice cover decreases significantly, causing the evaporation source to shift northward to cooler regions of the North Atlantic. As a result, both the atmospheric temperature over Greenland, T_G, and the extent of sea ice cover, C, influence the $\delta^{18}O$ signal. This justifies interpreting the signal I_G as a superposition of these two effects. Moreover, λ represents fast processes that are important for the evolution of sea ice; we hypothesize that it influences I_G in a manner similar to C. High values of λ, which correspond to extensive sea ice cover, are associated with larger temperature gradients between the site and the source. This results in a stronger negative effect on I_G, indicating lower temperatures.

III. SIMULATIONS

In this section, we give examples of simulations using the model introduced in Sec. II. We perform simulations of 30 kyr in length (taking benthic values from the period 120–90 kyr b2k) and start with fixed values of the subsurface water temperature in the North Atlantic T_{NAW}, to demonstrate different types of dynamical behavior within the model. The phase portraits in Fig. 4 show different dynamical behaviors dependent on the prescribed value of T_{NAW}, for short simulation runs. These correspond to "frozen" systems that can be used to understand the simulation of the full model shown with the NGRIP isotope record in Fig. 5, where T_{NAW} varies with time over the entire glacial period. At each time point during the glacial period, the behaviors are well approximated by the behavior of the frozen system.

In each of these phase portraits, a typical trajectory of (1)–(3) and (5) with noise is shown, superimposed onto the slow stable and unstable manifolds that correspond to trajectories of the singular system ($\epsilon \to 0$) in the noise-free case, $\sigma = 0$ in Eq. (5). In Figs. 4(c) and 4(d), we plot the stable limit cycles (obtained from a typical trajectory in the noise-free case) that change from a small oscillation around the unstable equilibrium to a large excursion along the three stable manifolds. For these demonstrations of different behavior, we purposely choose a lower noise amplitude than that used in Fig. 5. Figure 5 shows the NGRIP isotope record plotted against a stacked time series of all simulated variables of the system for a fixed noise level and T_{NAW} varying with time according to Eq. (2) in Sec. II. The noise level in Fig. 5 is chosen such that a realization of the entire glacial period produces a comparable number of DO events to that observed in the NGRIP record for visual comparison. For the phase portraits, we chose a lower noise amplitude and shorter simulation runs to visually demonstrate different types of behavior.

In the case $T_{NAW} = 0\,^{\circ}\mathrm{C}$ [Fig. 4(a)], the behavior of the trajectory is typical of the case before the first transition from interstadial to stadial phase. Due to the proximity of the C nullcline to the stable manifold, some realizations have exhibited slow and non-monotonic progression of C toward the fold bifurcation—it turns back on itself and may travel back down the stable manifold for a time before turning again. The cases $T_{NAW} = 10\,^{\circ}\mathrm{C}$ and $15\,^{\circ}\mathrm{C}$ [Figs. 4(b) and 4(c), respectively] show the consequences of loss of stability of an equilibrium close to the fold at the end of the upper branch. For the chosen noise amplitude, we find oscillations around the noise-free equilibrium that are Canard-like[63] in that they follow unstable parts of the critical manifold; for the higher T_{NAW} case, this can result in switching to the lower branch. The case $T_{NAW} = 20\,^{\circ}\mathrm{C}$ [Fig. 4(d)] shows a case where the oscillations around the noise-free equilibrium have disappeared and we have large amplitude relaxation oscillations corresponding to the repeated DO oscillations.

Figure 5 shows a comparison between the NGRIP oxygen isotope record and an example realization of all variables of the

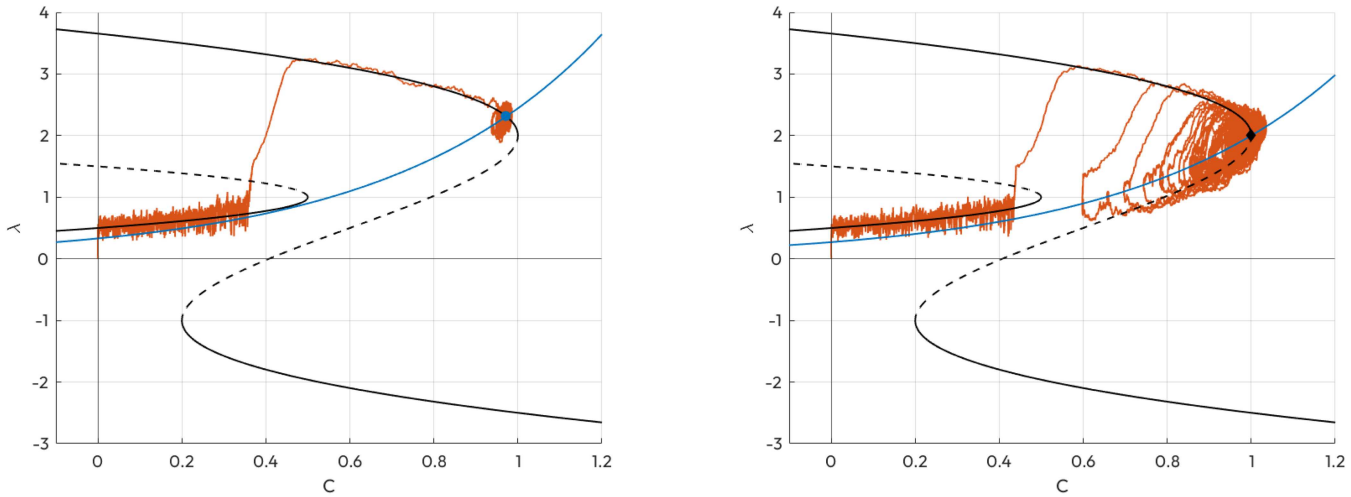

(a) $T_{NAW} = 0°C$ (b) $T_{NAW} = 10°C$

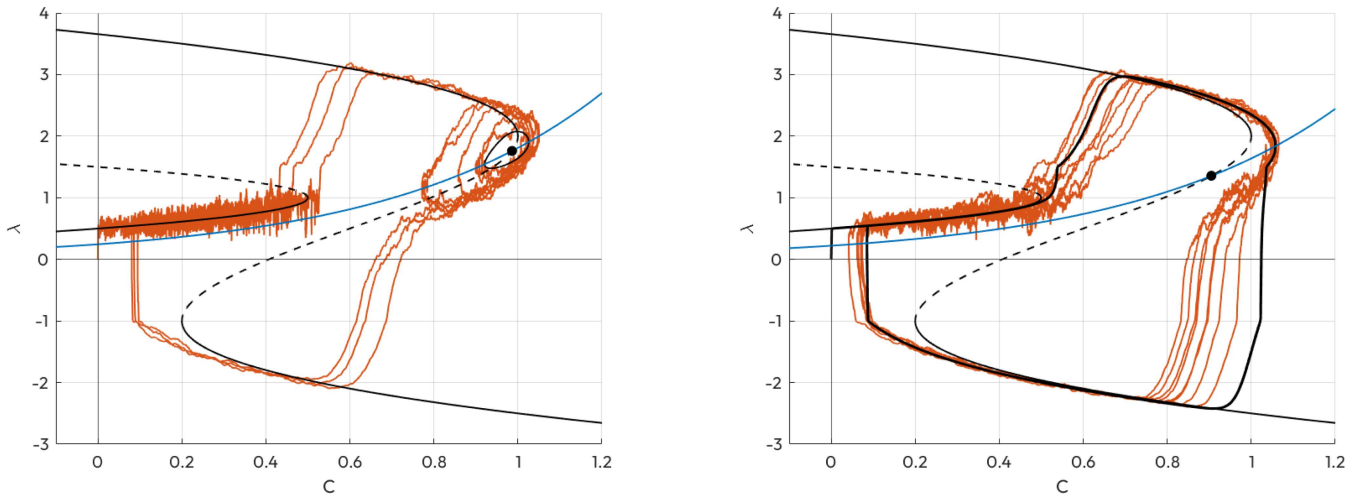

(c) $T_{NAW} = 15°C$ (d) $T_{NAW} = 20°C$

FIG. 4. Four fast–slow phase portraits in λ and C for trajectories with different fixed T_{NAW} values in the presence of noise $\sigma > 0$. (a) $T_{NAW} = 0\,°C$, (b) $T_{NAW} = 10\,°C$, (c) $T_{NAW} = 15\,°C$, (d) $T_{NAW} = 20\,°C$. Orange lines represent a trajectory of the system with initial condition $(C, \lambda) = (0, 0)$ and noise amplitude $\sigma = 0.1$. The black solid and dashed lines represent the stable and unstable slow manifolds, respectively. The speeds on the stable slow branches are prescribed by the function $h(\lambda, B, C)$ in Eq. (7). Blue lines represent a nullcline of C in the top equation of Eq. (5). (a) The nullcline intersects with the stable slow manifold, creating a stable fixed point denoted by a blue point; T_{NAW} is low, and there is an equilibrium near $C = 1$. (b) The nullcline intersects the fold bifurcation point, marked with a black diamond. At this value of T_{NAW}, the system is near a singular Hopf bifurcation. Noise induces oscillations near the full sea ice extent. (c) The intersection of the blue nullcline and the unstable manifold creates an unstable fixed point, marked with a black circle. In this regime, the system oscillates near full sea ice extent until it escapes to complete a full DO oscillation. (d) There is an unstable fixed point at the intersection of the nullcline and the unstable slow manifold, marked with a black point. The deterministic trajectory ($\sigma = 0$) is overlaid in black and is a large amplitude relaxation oscillation; the system shadows this in the presence of noise.

system over the entire glacial period, using T_{NAW} that changes with time as in Boers *et al.*[37] The system is able to replicate some of the sawtooth-shaped behavior seen in the NGRIP record and there is a rapid rise in temperature followed by varied rates of cooling during interstadials, with longer interstadials toward the beginning of the glacial period and shorter interstadials toward the middle and end of the glacial. Gray vertical lines in the panel (a) mark the observed DO events, consistent with that in Boers *et al.*,[37] and gray vertical lines in panel (b) mark where there has been a full oscillation in the simulation. A noise amplitude $\sigma = 0.15$ is used for the

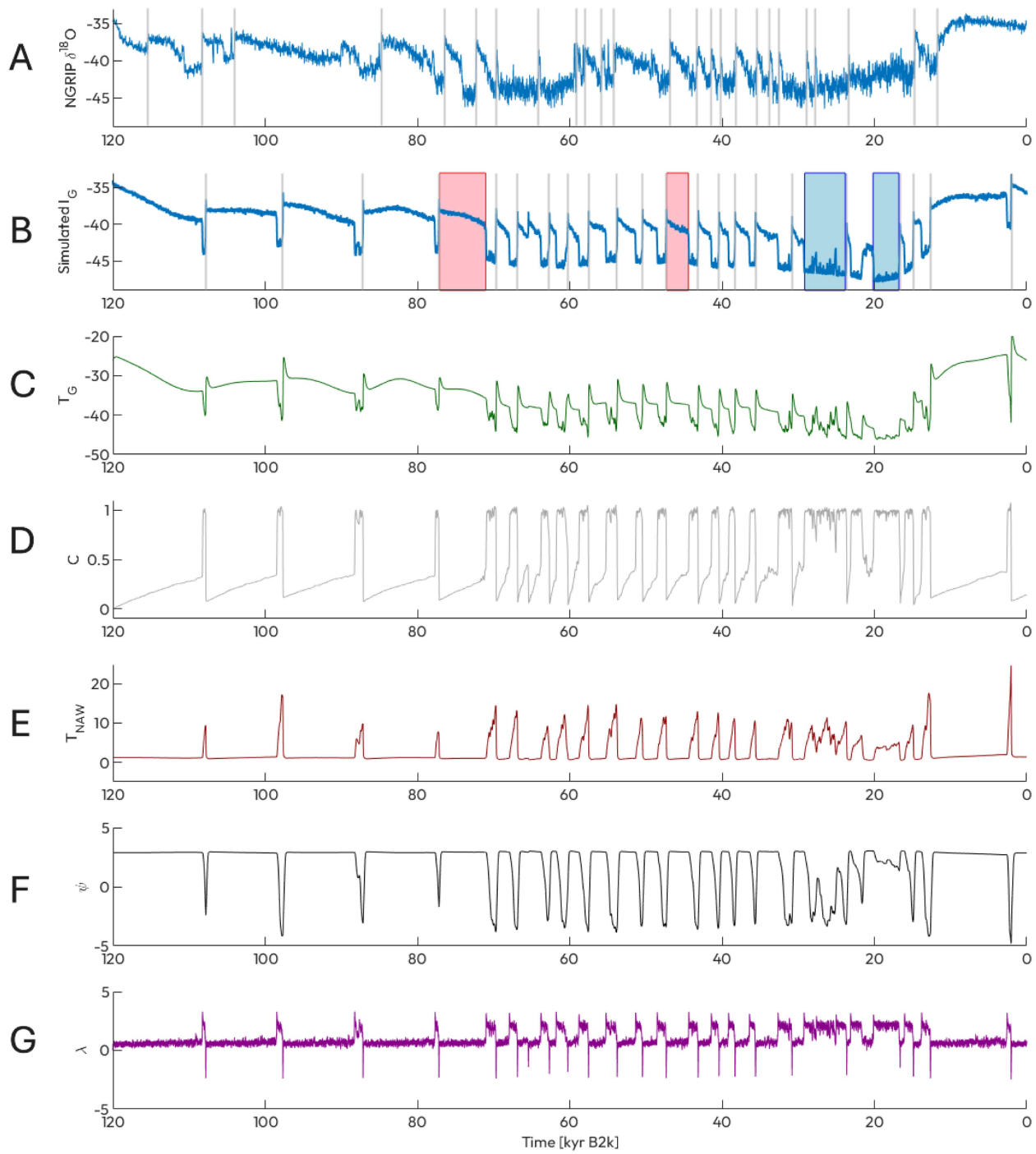

FIG. 5. The NGRIP record stacked with a model simulation for the last glacial period. (a) Observed time series of $\delta^{18}O$ obtained from the NGRIP record with 20 year mean sampling[62] (cyan). Gray vertical lines represent observed DO events. (b) Simulated time series of Greenland's NGRIP ice core using the conceptual model, $I_G(t)$ (cyan). Vertical gray lines indicate simulated DO events. Red and blue shaded regions, respectively, indicate interstadial and stadial periods that are tested for early warning signals in Figs. 6 and 7. (c) Atmospheric temperature over Greenland, $T_G(t)$ (green). (d) Sea ice extent in the North Atlantic, $C(t)$ (gray). (e) Subsurface water temperature in the North Atlantic, $T_{NAW}(t)$ (red). (f) AMOC strength anomaly, $\psi(t)$ (black). (g) Fast variable, $\lambda(t)$ (purple).

model simulation. The model simulation is run with a time step of $\Delta t = 0.1$ year. Note that the noise amplitude used here is larger than that of the simulations for fixed T_{NAW} in Fig. 4. At approximately 66 kyr b2k in the simulated isotope time series, there is an additional rapid warming event before the transition to stadial conditions. This is caused by noisy fluctuations kicking the system from the middle stable manifold back to the lower stable manifold (as opposed to the upper manifold). This feature looks similar to the jump observed at approximately 90 kyr b2k in the NGRIP record: an "unexpected" large increase in temperature before a more rapid cooling to stadial conditions. Another feature of the simulation includes a "half" DO event at approximately 22 kyr b2k. Here, we observe a large warming that does not progress into a full DO event. This corresponds to an excursion that travels along the unstable manifold for a long period of time before returning back to the upper stable manifold. It is important to note that depending on the noise level or parameters used to construct the fast–slow system [i.e., in Eq. (A1)] we may get more or fewer occurrences of these "atypical" DO-like events—but this is an interesting feature of the dynamical system and perhaps it could go some way to explain precursors for DO events. There is a larger observed standard deviation of $\delta^{18}O$ during stadials compared to interstadials.[64] This may be attributed to large-scale reorganizations of atmospheric circulation during stadial periods.[64,65] Indeed, a plausible interpretation of λ is that it includes large-scale atmospheric as well as oceanographic sea-ice processes. In simulations from the conceptual model we have presented here, a greater stadial variance is due to oscillatory behavior that arises as the subsurface water temperature T_{NAW} increases.

IV. EARLY WARNING SIGNALS OF ABRUPT SHIFTS IN THE MODEL

In this section, we examine signs of early warning preceding transitions from both interstadial to stadial and stadial to interstadial conditions. First, we present a method for sampling and detrending before calculating the early warning signals from the simulated isotope time series in Fig. 5.

The discretized simulated isotope time series in Fig. 5 (with a time step $\Delta t = 0.1$ year) is $I_i = I_G(t_i)$, where $t_{i+1} - t_i = \Delta t$ and $i = 1, \ldots, N_{tot}$. The finest resolution of the NGRIP ice core currently used for EWS analysis is sampled and interpolated at 5 year intervals[42] but does not capture all DO events that occurred during the last glacial period, as layer counting in the record stops at 60 kyr b2k.[66,67] Therefore, to align more closely with ice core records, we subsample our time series, I_i.

We define a subsampled time series, $\{y_i\}$, with time step $\Delta\tau = N_{sub}\Delta t$ and

$$y_i = \frac{1}{N_{sub}} \sum_{k=1}^{N_{sub}} I_{k+N_{sub}(i-1)},$$

for $i = 1, \ldots, \left\lfloor \frac{N_{tot}}{N_{sub}} \right\rfloor - N_{win} + 1$. We choose a sampling rate of $\Delta\tau = 5$ years (0.005 kyr) to have a similar resolution to an ice core record. Therefore, for an original time step of $\Delta t = 0.1$ year, we average over $N_{sub} = 50$ points.

For the calculation of the early warning signals, we use a sliding window over our time series, $\{y_i\}$. We define $N_{win} = 80$ to be the number of data points in our sliding window and, thus, the time duration of the sliding window is given by $\Delta w = N_{win}\Delta\tau = 400$ years.

Given the relatively short window, we remove only the mean from each window. So, the lth value in the jth window, $\tilde{y}_{l,j}$, is given by

$$\tilde{y}_{l,j} = y_{l+j-1} - \frac{1}{N_{win}} \sum_{k=1}^{N_{win}} y_{k+j-1}, \tag{9}$$

for $l = 1, \ldots, N_{win}$ and $j = 1, \ldots, \left\lfloor \frac{N_{tot}}{N_{sub}} \right\rfloor - N_{win} + 1$.

We can now construct an estimator[43] for the variance, $\{\hat{\nu}_j\}$, where

$$\hat{\nu}_j = \frac{1}{N_{win} - 1} \sum_{k=1}^{N_{win}} [\tilde{y}_{k,j}]^2,$$

for $j = 1, \ldots, \left\lfloor \frac{N_{tot}}{N_{sub}} \right\rfloor - N_{win} + 1$. Similarly, an estimator for the lag-1 (lag-$\Delta\tau$) autocorrelation is

$$\hat{\rho}_j = \frac{\sum_{k=1}^{N_{win}-1} [\tilde{y}_{k,j}\tilde{y}_{k+1,j}]}{\sqrt{\sum_{k=1}^{N_{win}-1} [\tilde{y}_{k,j}]^2} \sqrt{\sum_{k=1}^{N_{win}-1} [\tilde{y}_{k+1,j}]^2}},$$

for $j = 1, \ldots, \left\lfloor \frac{N_{tot}}{N_{sub}} \right\rfloor - N_{win} + 1$.

An expression for the standard deviation, σ_j of the estimator of the lag-1 autocorrelation is given by[43]

$$\sigma_j = \sqrt{\frac{2\hat{\rho}_j\Delta\tau}{N_{win}}}, \tag{10}$$

assuming that the underlying process is an Ornstein–Uhlenbeck (OU) process and $\hat{\rho}_j\Delta\tau$ is small.

The autocorrelation can be associated with a decay rate, α_j, that removes the dependency on the time step as

$$\alpha_j = -\frac{1}{\Delta\tau} \ln \hat{\rho}_j,$$

and the time series of the decay rate α is defined as $\alpha = \{\alpha_j\}$ for $j = 1, \ldots, \left\lfloor \frac{N_{tot}}{N_{sub}} \right\rfloor - N_{win} + 1$. Note that all $\hat{\rho}_j$ (and their error bounds) are greater than zero for suitably small $\Delta\tau$. Note that while the decay rate α_j is independent of the time step $\Delta\tau$, the estimator for the lag-1 autocorrelation, $\hat{\rho}_j$, depends on $\Delta\tau$.

We investigate the potential for early warning signals over both interstadial and stadial periods, namely, the onset and offset of DO events. In each of Figs. 6 and 7, we pick two interstadial and stadial periods as indicated by the red and blue shaded regions, respectively, in panel (b) of Fig. 5. The time series from the model simulation are repeated for the relevant period in the top panels. In the middle panels, we provide the sea ice cover extent C to indicate where the system is in the DO cycle. The bottom panels show the decay rate for each of the periods.

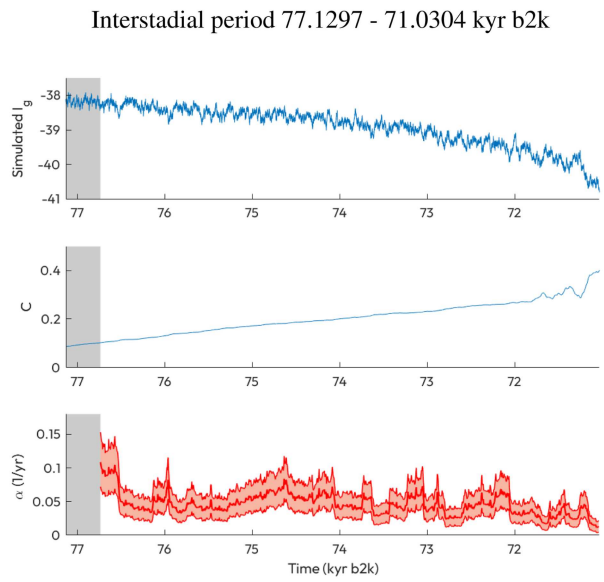

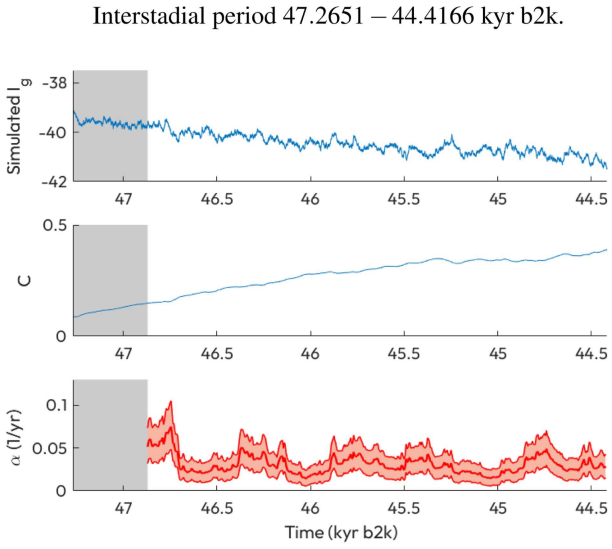

FIG. 6. Two examples of interstadial periods from model simulation, indicated by red shaded regions, presented in panel (b) of Fig. 5. (Top panels) Model simulation time series with time step $\Delta t = 0.1$ year (unsampled). At the end of the interstadial period, there is a rapid transition to stadial conditions. (Middle panels) Time series of sea ice extent C over the interstadial period. (Bottom panels) Evolution of α over the interstadial period, with sampling frequency 5 years, before the rapid transition to stadial conditions. Red shading indicates the variability in α after applying ± 1 standard deviation in lag-1 autocorrelation, given by Eq. (10). Gray shading in each panel indicated the size of the sliding window size used for the calculations, $\Delta w = 400$ years.

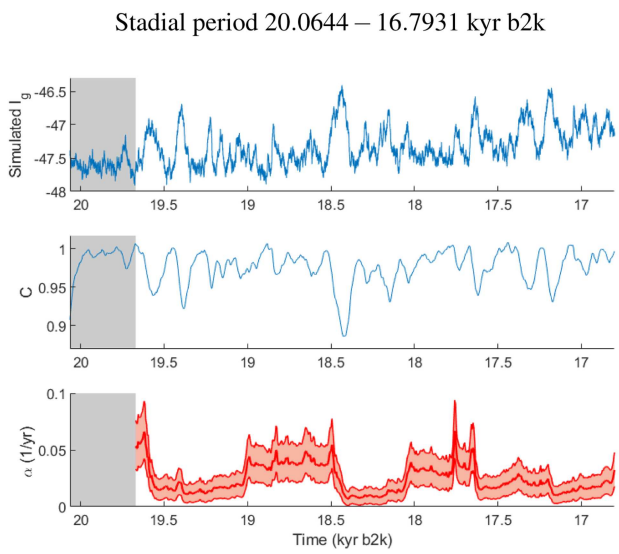

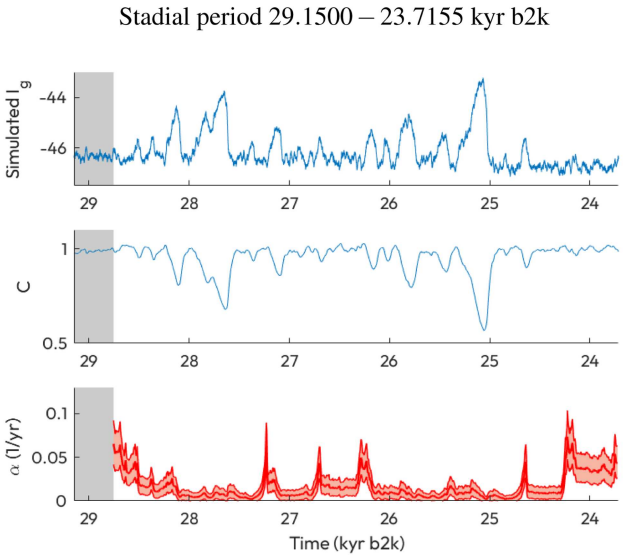

FIG. 7. Two examples of stadial periods from model simulation, indicated by red shaded regions, presented in panel (b) of Fig. 5. (Top panels) Model simulation time series with time step $\Delta t = 0.1$ year (unsampled). At the end of the stadial period, there is a rapid transition to interstadial conditions. (Middle panels) Time series of sea ice extent C over the stadial period. (Bottom panels) Evolution of α over the simulated stadial period before the rapid transition to interstadial conditions, with red shading indicates the variability in α after applying ± 1 standard deviation in lag-1 autocorrelation, given by Eq. (10). Gray shading in each panel indicated the size of the sliding window size used for the calculations, $\Delta w = 400$ years.

For the offset of a DO event (interstadial to stadial transition) in Fig. 6, we find a consistent decreasing trend in the decay rate from about 74.5 kyr b2k up to the transition at approximately 71 kyr b2k. Similarly, for the other interstadial period selected, there is a decreasing trend in the decay rate for the 3 kyr prior to the transition. This corresponds with the theory of critical slowing down for slowly approaching a fold bifurcation, e.g., Ashwin *et al.*,[44] Ditlevsen and Ditlevsen,[43] and Kuehn.[68] However, in both examples, we do

not observe a significant trend since the uncertainty band (representing the signal variability) always overlaps with itself (i.e., the upper boundary of the signal variability does not drop below the lower boundary) in the 3 kyr period prior to the transitions. We find this is the case for a number of choices of the parameters Δt, $\Delta\tau$, and Δw used to compute the EWS, but we do not present a detailed sensitivity analysis here.

For the DO onset examples in Fig. 7, we do not see a clear trend in the decay rate as the transition is approached. Moreover, the middle panel shows that the sea ice extent oscillates. Therefore, there is no clear linear increase (that is observed for the DO offset examples) in the approach to the transition. Hence, the decay rate, shown in the bottom panels, shows multiple increases and decreases prior to tipping, spoiling extrapolation.[44] We conjecture this is related to the presence of a singular Hopf bifurcation[69] upon the subsurface water temperature changing (T_{NAW}). As C slowly evolves close to the fold of the critical manifold, the eigenvalues become complex at a singular Hopf bifurcation in a neighborhood whose size scales with the timescale separation; see, for example, Kuehn[63] (Section 13.3).

To date, few studies have examined early warning signals in the context of Hopf bifurcations. Bury *et al.*[70] applied spectral EWS methods to a range of bifurcation types and demonstrated the ability to distinguish between oscillatory and non-oscillatory bifurcations. While this work makes progress in characterizing bifurcation types, there remains a lack of early warning signals specifically tailored to singular Hopf bifurcations.[69] Future work is needed to address this gap in effective EWS for bifuractions that appear in the singular limit. Figure 7 shows that in many cases looking for evidence of tipping with variance and lag-1 autocorrelation may not be enlightening, especially when it cannot be confirmed that the mechanism behind the tipping is a fold bifurcation in a slowly varying subsystem or whether the extrapolation is valid.[44]

V. DISCUSSION

Regularizing a continuous-time dynamical system with instantaneous switching[39,55] creates a system that limits to the switching system as some timescale ratio limits to zero. This is a singular limit as the switching system is no longer a differential equation. In this paper, we do this for the model of Boers *et al.* of the Dansgaard–Oeschger events[37] although clearly there is no unique regularization, it is reasonable to assume that they will reflect similar behavior in the singular limit.

We do not attempt to correct issues with the model of Boers *et al.*[37], though this would be possible. With an increasing number of Earth system models reaching the complexity to reproduce DO-like events,[20,29] will present opportunities for improved conceptual modeling, validated against ESMs and proxy records. A key aspect of this will be to understand the physical mechanisms that determine amplitude and characteristics (such as correlations, intermittency, and state-dependence) of the natural variability.

To regularize the switching model, we propose that there is a fast dynamic process $\lambda(t)$ that switches between three different stable branches. This represents the three possible modes of evolutions of total sea ice extent $C(t)$ in Boers *et al.*[37] The fast process λ parametrizes processes that govern sea ice growth and decay in order to regularize the switching behavior expressed as (4) in Boers *et al.*[37] As such it includes information about the robustness of the ice shelf such as buttressing and ice thickness. The functional form of the equation for the λ dynamics (see Appendix A) is constrained by the interconnection of the branches at switching but leaves many details open to choice. The branches interconnect similarly to the switching model of Paillard[71] for the Pleistocene ice-age cycle, which has been regularized in Ashwin and Ditlevsen.[72] However, the dynamics on the three branches in our model have different timescales as illustrated in Fig. 2. The λ dynamics is assumed faster than timescales of C on each of the branches, as determined by Eq. (5).

This approach is successful in that it can produce comparable statistics to Boers *et al.*[37] for the timing of DO events in response to the non-autonomous driving from a proxy benthic record of the global climate state. It attributes the stochastic variability to stochastic differential equations that govern the fast–slow system, rather than introducing observational noise.[37] This means there is the potential for the system to show early warning signals of approaching tipping points in a fast system. We note that the abrupt changes in the model of Boers *et al.* have a different mechanism to studies such as de Verdière[14] and Sévellec and Fedorov.[15,16] These assign relatively rapid changes to a salinity feedback mechanism that does not rely on interaction with the ice sheet.

We examine examples of onset and offset of interstadials for evidence of EWS. The comparatively rapid dynamics of λ are challenging for this—indeed, for the chosen noise and parameters, we find cases where there is very little warning evident. This is despite regularizing the model to have abrupt transitions caused by instabilities rather than artificial switches. We conjecture that the presence of a singular Hopf bifurcation[69] is an obstruction to reliable EWS. Different methods for calculating EWS and significance testing (e.g., Ben-Yami *et al.*[73]) may provide different conclusions. Note that EWS need to have a relevant observable to have any chance of a skillful prediction[45,74] and may be obscured by using other types of noise such as alpha-stable Levy noise.[31,32]

ACKNOWLEDGMENTS

Thanks to Niklas Boers, Peter Ditlevsen, John Slattery, and Louise Sime for stimulating conversations related to this work. We thank the reviewers and Georg Gottwald for their insightful comments. For the purpose of open access, the authors have applied a Creative Commons Attribution (CC BY) licence to any Author Accepted Manuscript version arising from this submission. P.D.L.R. and P.A. were supported by the European Union's Horizon Europe Research and Innovation Programme under Grant Agreement No. 101137601 (ClimTip). P.D.L.R. also acknowledges the Optimal High Resolution Earth System Models for Exploring Future Climate Changes (OptimESM) project, Grant Agreement No. 101081193.

AUTHOR DECLARATIONS

Conflict of Interest

Yes, one of the authors (PA) is a guest editor for the issue.

Author Contributions

Bryony Hobden: Investigation (lead); Methodology (equal); Visualization (lead); Writing – original draft (equal); Writing – review & editing (lead). **Peter Ashwin:** Investigation (supporting); Methodology (equal); Supervision (equal); Writing – original draft (equal); Writing – review & editing (supporting). **Paul D. L. Ritchie:** Investigation (supporting); Methodology (supporting); Supervision (equal); Writing – original draft (equal); Writing – review & editing (supporting).

DATA AVAILABILITY

The code that generates the data in support of the findings of this study is openly available in GitHub at https://github.com/Bryony-Hobden/DO-EWS-code, Ref. 75.

APPENDIX A: DERIVATION OF EQUATION FOR λ DYNAMICS

We choose g to be a fifth-order polynomial in C and λ that has

- A hysteresis loop between stable branches at high and low values of λ corresponding to rapidly growing and retreating sea-ice states. This has one-fold bifurcation at $C \approx 0$ and one at C small but close to zero.
- There is an additional stable branch for low C that ends at a fold bifurcation at $C = 0.5$.
- There are no intersections between these branches on exit from the folds the transitions are as in the model of Ref. 37.

$$g(\lambda, C) = \left(-\frac{8\lambda^3}{135} + \frac{4\lambda^2}{45} + \frac{16\lambda}{45} + \frac{11}{27} - C\right) \times \left(2(\lambda - \frac{1}{2})(\lambda - \frac{3}{2}) + C\right). \quad \text{(A1)}$$

APPENDIX B: REGULARIZED MODEL PARAMETER VALUES

Table I lists parameters and the values used in the regularized model consisting of Eqs. (1)–(3) and (5)–(8).

TABLE I. Table of parameters used in the regularized model.

Parameter	Value (units)	Description
p_0	5.56 (kyr^{-1})	Inverse timescale of temperature variables
τ	10 (°C)	Critical threshold in T_{NAW} for sea ice growth
ϵ	0.01 (kyr)	Timescale separation between λ and C
σ	0.15 (—)	Noise amplitude on λ
β	1 (—)	Scaling parameter between λ and I_G

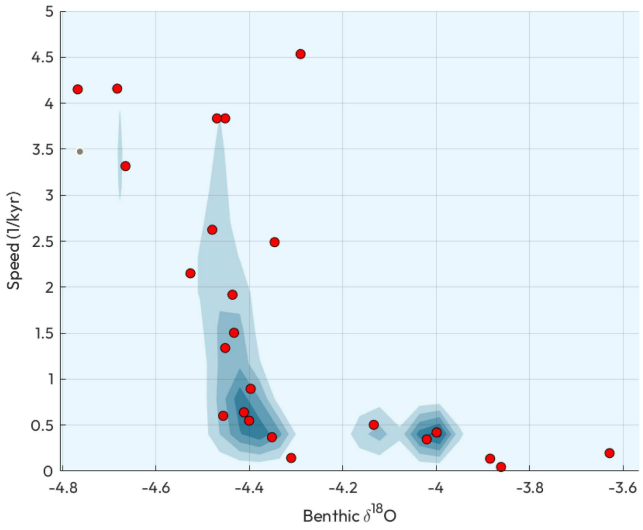

FIG. 8. Two-dimensional Gaussian kernel density estimate of the joint probability density function (PDF) of the speed at which the Greenland ice shelf grows—taken as the inverse of the interstadial duration—and the benthic δ^{18}O. The red circles denote the observed values. From this KDE, 99 PDFs were calculated corresponding to a range of 99 evenly distributed benthic δ^{18}O values. The function $f(B)$ takes the current value of benthic δ^{18}O and identifies the closest benthic value from the array and samples from the corresponding PDF to produce a sea ice growth speed.

APPENDIX C: KERNEL DENSITY ESMIMATE

Figure 8 illustrates the kernel density estimate used to generate values of $f(B)$ and details how it is used in determining sea ice growth speed—see Boers *et al.*[37]

REFERENCES

[1] W. Dansgaard, H. B. Clausen, N. Gundestrup, C. U. Hammer, S. F. Johnsen, P. Kristinsdottir, and N. Reeh, "A new Greenland deep ice core," Science **218**, 1273–1277 (1982).
[2] W. Dansgaard, S. J. Johnsen, H. B. Clausen, D. Dahl-Jensen, N. Gundestrup, C. U. Hammer, and H. Oeschger, "North Atlantic climatic oscillations revealed by deep Greenland ice cores," in *Climate Processes and Climate Sensitivity*, Geophysical Monograph Series, edited by J. E. Hansen and T. Takahashi (AGU, 1984).
[3] S. Johnsen, H. Clausen, D. Dahl-Jensen, C. Hammer, C. Hvidberg, J. Steffensen, W. Dansgaard, N. Gundestrup, A. Sveinbjornsdottir, J. Jouzel, and G. Bond, "Evidence for general instability of past climate from a 250-kyr ice-core record," Nature **364**, 218–220 (1993).
[4] S. J. Johnsen, H. B. Clausen, W. Dansgaard, K. Fuhrer, N. Gundestrup, C. U. Hammer, P. Iversen, J. Jouzel, B. Stauffer, and J. P. Steffensen, "Irregular glacial interstadials recorded in a new Greenland ice core," Nature **359**, 311–313 (1992).
[5] W. S. Broecker, D. M. Peteet, and D. Rind, "Does the ocean–atmosphere system have more than one stable mode of operation?" Nature **315**, 21–26 (1985).
[6] L. C. Menviel, L. C. Skinner, L. Tarasov, and P. C. Tzedakis, "An ice–climate oscillatory framework for Dansgaard–Oeschger cycles," Nat. Rev. Earth Environ. **1**, 677–693 (2020).
[7] A. H. Voelker, "Global distribution of centennial-scale records for Marine Isotope Stage (MIS) 3: A database," Quat. Sci. Rev. **21**, 1185–1212 (2002).

[8]P. Kindler, M. Guillevic, M. Baumgartner, J. Schwander, A. Landais, and M. Leuenberger, "Temperature reconstruction from 10 to 120 kyr b2k from the NGRIP ice core," Clim. Past **10**, 887–902 (2014).
[9]K. Andersen, N. Azuma, J. Barnola, M. Bigler, P. Biscaye, N. Caillon, J. Chappellaz, H. Clausen, D. Dahl-Jensen, H. Fischer *et al.*, "High-resolution record of Northern Hemisphere climate extending into the last interglacial period," Nature **431**, 147–151 (2004).
[10]L. E. Lisiecki and M. E. Raymo, "A Pliocene-Pleistocene stack of 57 globally distributed benthic $\delta^{18}O$ records," Paleoceanography **20**, PA1003 (2005).
[11]P. Welander, "Thermohaline effects in the ocean circulation and related simple models," in *Large-Scale Transport Processes in Oceans and Atmosphere* (Springer, 1986), pp. 163–200.
[12]C. Wunsch, "Thermohaline loops, Stommel box models, and the Sandström theorem," Tellus A: Dyn. Meteorol. Oceanogr. **57**, 84–99 (2005).
[13]T. F. Stocker and S. J. Johnsen, "A minimum thermodynamic model for the bipolar seesaw," Paleoceanography **18**, 1087 (2003).
[14]A. C. de Verdière, "A simple model of millennial oscillations of the thermohaline circulation," J. Phys. Oceanogr. **37**, 1142–1155 (2007).
[15]F. Sévellec and A. V. Fedorov, "Millennial variability in an idealized ocean model: Predicting the AMOC regime shifts," J. Clim. **27**, 3551–3564 (2014).
[16]F. Sévellec and A. V. Fedorov, "Unstable AMOC during glacial intervals and millennial variability: The role of mean sea ice extent," Earth Planet. Sci. Lett. **429**, 60–68 (2015).
[17]A. C. de Verdière and L. Te Raa, "Weak oceanic heat transport as a cause of the instability of glacial climates," Clim. Dyn. **35**, 1237–1256 (2010).
[18]O. Arzel, A. C. de Verdière, and M. H. England, "The role of oceanic heat transport and wind stress forcing in abrupt millennial-scale climate transitions," J. Clim. **23**, 2233–2256 (2010).
[19]I. Eisenman, C. M. Bitz, and E. Tziperman, "Rain driven by receding ice sheets as a cause of past climate change," Paleoceanography **24**(4), PA4209 (2009).
[20]I. Malmierca-Vallet, L. C. Sime, andThe D-O Community Members, "Dansgaard–Oeschger events in climate models: Review and baseline Marine Isotope Stage 3 (MIS3) protocol," Clim. Past **19**, 915–942 (2023).
[21]G. Vettoretti and W. R. Peltier, "Fast physics and slow physics in the nonlinear Dansgaard–Oeschger relaxation oscillation," J. Clim. **31**, 3423–3449 (2018).
[22]T. M. Dokken, K. H. Nisancioglu, C. Li, D. S. Battisti, and C. Kissel, "Dansgaard-Oeschger cycles: Interactions between ocean and sea ice intrinsic to the Nordic seas," Paleoceanography **28**, 491–502 (2013).
[23]H. Sadatzki, N. Maffezzoli, T. M. Dokken, M. H. Simon, S. M. P. Berben, K. Fahl, H. A. Kjær, A. Spolaor, R. Stein, P. Vallelonga, B. M. Vinther, and E. Jansen, "Rapid reductions and millennial-scale variability in Nordic seas sea ice cover during abrupt glacial climate changes," Proc. Natl. Acad. Sci. **117**, 29478–29486 (2020).
[24]E. Armstrong, K. Izumi, and P. Valdes, "Identifying the mechanisms of DO-scale oscillations in a GCM: A salt oscillator triggered by the laurentide ice sheet," Clim. Dyn. **60**, 3983–4001 (2023).
[25]Y. Kuniyoshi, A. Abe-Ouchi, S. Sherriff-Tadano, W.-L. Chan, and F. Saito, "Effect of climatic precession on Dansgaard-Oeschger-like oscillations," Geophys. Res. Lett. **49**, e2021GL095695, https://doi.org/10.1029/2021GL095695 (2022).
[26]X. Zhang, S. Barker, G. Knorr, G. Lohmann, R. Drysdale, Y. Sun, D. Hodell, and F. Chen, "Direct astronomical influence on abrupt climate variability," Nat. Geosci. **14**, 819–826 (2021).
[27]N. Wunderling, A. S. von der Heydt, Y. Aksenov, S. Barker, R. Bastiaansen, V. Brovkin, M. Brunetti, V. Couplet, T. Kleinen, C. H. Lear *et al.*, "Climate tipping point interactions and cascades: A review," Earth Syst. Dyn. **15**, 41–74 (2024).
[28]W. R. Peltier and G. Vettoretti, "Dansgaard-Oeschger oscillations predicted in a comprehensive model of glacial climate: A "kicked" salt oscillator in the Atlantic," Geophys. Res. Lett. **41**, 7306–7313, https://doi.org/10.1002/2014GL061413 (2014).
[29]G. Vettoretti and W. R. Peltier, "Thermohaline instability and the formation of glacial North Atlantic super polynyas at the onset of Dansgaard-Oeschger warming events," Geophys. Res. Lett. **43**, 5336–5344, https://doi.org/10.1002/2016GL068891 (2016).
[30]G. Vettoretti, P. Ditlevsen, M. Jochum, and S. O. Rasmussen, "Atmospheric CO_2 control of spontaneous millennial-scale ice age climate oscillations," Nat. Geosci. **15**, 300–306 (2022).
[31]K. Riechers, G. Gottwald, and N. Boers, "Glacial abrupt climate change as a multiscale phenomenon resulting from monostable excitable dynamics," J. Clim. **37**, 2741–2763 (2024).
[32]G. A. Gottwald, "A model for Dansgaard–Oeschger events and millennial-scale abrupt climate change without external forcing," Clim. Dyn. **56**, 227–243 (2021).
[33]A. Timmermann, H. Gildor, M. Schulz, and E. Tziperman, "Coherent resonant millennial-scale climate oscillations triggered by massive meltwater pulses," J. Clim. **16**, 2569–2585 (2003).
[34]H. A. Singh, D. S. Battisti, and C. M. Bitz, "A heuristic model of Dansgaard–Oeschger cycles. Part I: Description, results, and sensitivity studies," J. Clim. **27**, 4337–4358 (2014).
[35]J. O. Melcher, S. Halkjær, P. Ditlevsen, P. L. Langen, G. Vettoretti, and S. O. Rasmussen, "A novel conceptual model for Dansgaard–Oeschger event dynamics based on ice-core data," Clim. Past **21**, 115–132 (2025).
[36]M. Schulz, A. Paul, and A. Timmermann, "Relaxation oscillators in concert: A framework for climate change at millennial timescales during the late pleistocene," Geophys. Res. Lett. **29**, 46-1–46-4, https://doi.org/10.1029/2002GL016144 (2002).
[37]N. Boers, M. Ghil, and D.-D. Rousseau, "Ocean circulation, ice shelf, and sea ice interactions explain Dansgaard–Oeschger cycles," Proc. Natl. Acad. Sci. **115**, E11005–E11014 (2018).
[38]J. Fohlmeister, N. Sekhon, A. Columbu, G. Vettoretti, N. Weitzel, K. Rehfeld, C. Veiga-Pires, M. Ben-Yami, N. Marwan, and N. Boers, "Global reorganization of atmospheric circulation during Dansgaard–Oeschger cycles," Proc. Natl. Acad. Sci. **120**, e2302283120 (2023).
[39]M. R. Jeffrey, *Modeling with Nonsmooth Dynamics*, Frontiers in Applied Dynamical Systems: Reviews and Tutorials (Springer, 2020).
[40]M. Scheffer, J. Bascompte, W. A. Brock, V. Brovkin, S. R. Carpenter, V. Dakos, H. Held, E. H. Van Nes, M. Rietkerk, and G. Sugihara, "Early-warning signals for critical transitions," Nature **461**, 53–59 (2009).
[41]V. Dakos, M. Scheffer, E. H. Van Nes, V. Brovkin, V. Petoukhov, and H. Held, "Slowing down as an early warning signal for abrupt climate change," Proc. Natl. Acad. Sci. **105**, 14308–14312 (2008).
[42]N. Boers, "Early-warning signals for Dansgaard-Oeschger events in a high-resolution ice core record," Nat. Commun. **9**, 2556 (2018).
[43]P. Ditlevsen and S. Ditlevsen, "Warning of a forthcoming collapse of the Atlantic Meridional Overturning Circulation," Nat. Commun. **14**, 4254 (2023).
[44]P. Ashwin, R. Bastiaansen, A. S. von der Heydt, and P. Ritchie, "Early warning skill, extrapolation and tipping for accelerating cascades," arXiv:2506.01981 [nlin.CD] (2025).
[45]J. Lohmann, A. B. Hansen, A. Lovo, R. Chapman, F. Bouchet, and V. Lucarini, "The role of edge states for early-warning of tipping points," Proc. R. Soc. A **481**, 20240753 (2025).
[46]M. Rypdal, "Early-warning signals for the onsets of Greenland interstadials and the Younger Dryas–Preboreal transition," J. Clim. **29**, 4047–4056 (2016).
[47]T. Mitsui and N. Boers, "Statistical precursor signals for Dansgaard–Oeschger cooling transitions," Clim. Past **20**, 683–699 (2024).
[48]J. Lohmann, "Prediction of Dansgaard-Oeschger events from Greenland dust records," Geophys. Res. Lett. **46**, 12427–12434, https://doi.org/10.1029/2019GL085133 (2019).
[49]A. Cimatoribus, S. Drijfhout, V. Livina, and G. Van Der Schrier, "Dansgaard–Oeschger events: Bifurcation points in the climate system," Clim. Past **9**, 323–333 (2013).
[50]P. D. Ditlevsen and S. J. Johnsen, "Tipping points: Early warning and wishful thinking," Geophys. Res. Lett. **37**, L19703, https://doi.org/10.1029/2010GL044486 (2010).
[51]A. C. de Verdiere, M. B. Jelloul, and F. Sévellec, "Bifurcation structure of thermohaline millennial oscillations," J. Clim. **19**, 5777–5795 (2006).
[52]F. Sévellec, T. Huck, and A. C. de Verdiere, "From centennial to millennial oscillation of the thermohaline circulation," J. Mar. Res. **68**, 723–742 (2010).
[53]M. Winton, "Deep decoupling oscillations of the oceanic thermohaline circulation," in *Ice in the Climate System* (Springer, 1993), pp. 417–432.
[54]M. Winton, "Energetics of deep-decoupling oscillations," J. Phys. Oceanogr. **25**, 420–427 (1995).
[55]D. D. Novaes and M. R. Jeffrey, "Regularization of hidden dynamics in piecewise smooth flows," J. Differ. Eq. **259**, 4615–4633 (2015).

[56]P. Cessi, "A simple box model of stochastically forced thermohaline flow," J. Phys. Oceanogr. **24**, 1911–1920 (1994).
[57]H. Stommel, "Thermohaline convection with two stable regimes of flow," Tellus **13**, 224–230 (1961).
[58]E. Süli and D. F. Mayers, *An Introduction to Numerical Analysis* (Cambridge University Press, 2003).
[59]J. Jouzel, G. Hoffmann, R. Koster, and V. Masson, "Water isotopes in precipitation: Data/model comparison for present-day and past climates," Quat. Sci. Rev. **19**, 363–379 (2000).
[60]H. C. Steen-Larsen, "Continuous monitoring of summer surface water vapor-isotopic composition above the Greenland ice sheet," Atmos. Chem. Phys. **13**, 4815–4828 (2013).
[61]V. Masson-Delmotte, "GRIP deuterium excess reveals rapid and orbital-scale changes in Greenland moisture origin," Science **309**, 118–121 (2005).
[62]S. O. Rasmussen, M. Bigler, S. P. Blockley, T. Blunier, S. L. Buchardt, H. B. Clausen, I. Cvijanovic, D. Dahl-Jensen, S. J. Johnsen, H. Fischer, V. Gkinis, M. Guillevic, W. Z. Hoek, J. J. Lowe, J. B. Pedro, T. Popp, I. K. Seierstad, J. P. Steffensen, A. M. Svensson, P. Vallelonga, B. M. Vinther, M. J. Walker, J. J. Wheatley, and M. Winstrup, "A stratigraphic framework for abrupt climatic changes during the last glacial period based on three synchronized Greenland ice-core records: Refining and extending the intimate event stratigraphy," Quat. Sci. Rev. **106**, 14–28 (2014), Dating, Synthesis, and Interpretation of Palaeoclimatic Records and Model-data Integration: Advances of the INTIMATE project (INTegration of Ice core, Marine and TErrestrial records, COST Action ES0907).
[63]C. Kuehn, *Multiple Time Scale Dynamics*, 2015th ed., Applied Mathematical Sciences (Springer International Publishing, Cham, 2015).
[64]P. D. Ditlevsen, S. Ditlevsen, and K. K. Andersen, "The fast climate fluctuations during the stadial and interstadial climate states," Ann. Glaciol. **35**, 457–462 (2002).
[65]T. Erhardt, E. Capron, S. O. Rasmussen, S. Schüpbach, M. Bigler, F. Adolphi, and H. Fischer, "Decadal-scale progression of the onset of Dansgaard–Oeschger warming events," Clim. Past **15**, 811–825 (2019).
[66]North Greenland Ice Core Project members, "High-resolution record of Northern Hemisphere climate extending into the last interglacial period," Nature **431**, 147–151 (2004).
[67]V. Gkinis, S. B. Simonsen, S. L. Buchardt, J. White, and B. M. Vinther, "Water isotope diffusion rates from the NorthGRIP ice core for the last 16 000 years—Glaciological and paleoclimatic implications," Earth Planet. Sci. Lett. **405**, 132–141 (2014).
[68]C. Kuehn, "A mathematical framework for critical transitions: Bifurcations, fast–slow systems and stochastic dynamics," Physica D **240**, 1020–1035 (2011).
[69]S. Baer and T. Erneux, "Singular Hopf bifurcation to relaxation oscillations," SIAM J. Appl. Math. **46**(5), 721–739 (1986).
[70]T. M. Bury, C. T. Bauch, and M. Anand, "Detecting and distinguishing tipping points using spectral early warning signals," J. R. Soc. Interface **17**, 20200482 (2020).
[71]D. Paillard, "The timing of Pleistocene glaciations from a simple multiple-state climate model," Nature **391**, 378–381 (1998).
[72]P. Ashwin and P. Ditlevsen, "The middle Pleistocene transition as a generic bifurcation on a slow manifold," Clim. Dyn. **45**, 2683–2695 (2015).
[73]M. Ben-Yami, A. Morr, S. Bathiany, and N. Boers, "Uncertainties too large to predict tipping times of major earth system components from historical data," Sci. Adv. **10**, eadl4841 (2024).
[74]A. Morr, N. Boers, and P. Ashwin, "Internal noise interference to warnings of tipping points in generic multidimensional dynamical systems," SIAM J. Appl. Dyn. Syst. **23**, 2793–2806 (2024).
[75]Dataset: B. Hobden (2025). "DO-EWS-code," Zenodo. https://doi.org/10.5281/zenodo.16633153.